

# Dust and gas in luminous infrared galaxies - results from SCUBA observations

U. Lisenfeld<sup>1</sup>, K.G. Isaak<sup>2\*</sup>, R. Hills<sup>3</sup>

<sup>1</sup>*IRAM, Avenida Divina Pastora 7, N.C., 18012 Granada, Spain, e-mail: ute@iram.es*

<sup>2</sup>*Department of Astronomy, University of Maryland, College Park, USA*

<sup>3</sup>*Cavendish Astrophysics Group, Cavendish Laboratory, Madingley Road, Cambridge CB3 0HE, UK*

10 May 2018

## ABSTRACT

We present new data taken at 850  $\mu\text{m}$  with SCUBA at the JCMT for a sample of 19 luminous infrared galaxies. Fourteen galaxies were detected. We have used these data, together with fluxes at 25, 60 and 100  $\mu\text{m}$  from IRAS, to model the dust emission. We find that the emission from most galaxies can be described by an optically thin, single temperature dust model with an exponent of the dust extinction coefficient ( $k_\lambda \propto \lambda^{-\beta}$ ) of  $\beta \simeq 1.4 - 2$ . A lower  $\beta \simeq 1$  is required to model the dust emission from two of the galaxies, Arp 220 and NGC 4418. We discuss various possibilities for this difference and conclude that the most likely is a high dust opacity. In addition, we compare the molecular gas mass derived from the dust emission,  $M_{850\mu\text{m}}$ , with the molecular gas mass derived from the CO emission,  $M_{\text{CO}}$ , and find that  $M_{\text{CO}}$  is on average a factor 2–3 higher than  $M_{850\mu\text{m}}$ .

**Key words:** dust, extinction – ISM: molecules – galaxies: ISM – galaxies: starburst

## 1 INTRODUCTION

Much observational evidence has been accumulated since the first discovery of luminous (infrared luminosities of  $L_{\text{IR}} = L(8 - 1000\mu\text{m}) > 10^{11} L_\odot$ , “LIRGs”) and ultraluminous ( $L_{\text{IR}} > 10^{12} L_\odot$ , “ULIRGs”) infrared galaxies to suggest that their interstellar medium (ISM) is quite different from that of normal galaxies. ULIRGs and LIRGs contain very large quantities of molecular gas, as traced by CO (e.g. Sanders et al. 1988), and by tracers of high density gas such as HCN and CS(3-2) (Solomon, Downes & Radford 1992). In spite of their abundance of molecular hydrogen, LIRGs have ratios of far-infrared (FIR) luminosity to molecular gas mass,  $L_{\text{FIR}}/M_{\text{H}_2}$ , that largely exceed those measured in our own galaxy (Solomon et al. 1992). The ratio between the luminosity of the high-density tracers and  $L_{\text{FIR}}$ , however, is quite normal. The FIR emission is a measure of the star formation activity in a galaxy and so the constant  $L_{\text{FIR}}/L_{\text{HCN}}$  implies that the star formation rate (SFR) per *dense* gas mass is normal. The ratio of the luminosity of the high-density gas tracers to CO is much higher than in our own galaxy, and so it would appear that a larger fraction of the molecular gas is in a dense state. Solomon et al. (1997) conclude from this that the ISM of ULIRGs is much denser than

in normal galaxies, with even gas in intercloud regions being in the molecular state.

The dust properties of LIRGS are also different from those found in less luminous galaxies. There are a number of strong indications that the dust opacity in LIRGs is very high, with the result that the emission from LIRGs is optically thick even in the FIR wavelength range. Based on the tight correlation between the flux at 100  $\mu\text{m}$  and the CO emission of ULIRGs, Solomon et al. (1997) argue that the ISM is optically thick at wavelengths as long as 100  $\mu\text{m}$ . A high opacity in Arp 220 is supported by a range of observations: (i) Emerson et al. (1984) have concluded from observations in the IR and submillimetre that the dust opacity is of order unity between 100 and 200  $\mu\text{m}$ . (ii) From observations with ISO using the Long Wavelength Spectrometer (LWS) Fischer et al. (1997) derived unity optical depth at  $\simeq 150\mu\text{m}$ . (iii) The ratios of the IR fine structure line emission observed by ISO (Genzel et al. 1998) are consistent with a screen opacity of  $A_V \simeq 45$  mag, equivalent to an opacity of  $A_V \simeq 1000$  mag if the dust and gas were well-mixed. (iv) Calculations by Downes & Solomon (1998) using measurements of the CO surface brightness and a galactic dust-to-gas ratio suggest an opacity of about  $A_V \simeq 1000$  mag. The dust opacity is also high in NGC 4418, where a high dust extinction has been measured at optical wavelengths ( $A_V \gg 50$  mag, Roche et al. 1986). The high dust opacity might also explain why the  $\text{C}^+$  158  $\mu\text{m}$  line is so weak in ULIRGs (Malhorta et al. 1997, Luhman et al. 1998).

\* Now at Cavendish Astrophysics Group, Cavendish Laboratory, Madingley Road, Cambridge CB3 0HE, UK, e-mail: isaak@mrao.cam.ac.uk

An accurate measurement of the molecular gas mass of a galaxy is critical to determining star formation activity. Estimating the molecular gas mass of an object is not straightforward, and is typically made in one of two ways: The first method relies on observations of the optically thick CO(1-0) emission. The calculated CO line luminosity can be converted to a H<sub>2</sub> gas mass by adopting a conversion factor between CO and H<sub>2</sub> that has been derived from observations of Galactic molecular clouds (e.g. Young & Scoville 1982) and  $\gamma$ -rays fluxes (Bloemen et al. 1986). The second method makes use of the empirical relationship between gas and dust mass. The dust mass can be determined from the dust emission spectrum with assumptions made about the dust emissivity and composition. The dust mass can in turn be converted into a molecular gas mass using the locally derived gas-to-dust mass ratio (e.g. Hildebrand 1983).

Both derivations assume that the dust and gas parameters derived from measurements in our own galaxy are valid under the quite different conditions in LIRGs, and that they are independent of star formation activity. Theoretical arguments by Maloney & Black (1988) suggest that the CO-to-H<sub>2</sub> conversion factor should be considerably lower in actively star forming galaxies because of the higher density and temperature of the constituent molecular clouds. Observationally, there are also indications that the Galactic CO-to-H<sub>2</sub> conversion factor overestimates the molecular gas mass in LIRGs: Shier, Rieke & Rieke (1994) find that the molecular gas mass derived from CO emission using the standard Galactic conversion factor exceeds the dynamical mass by a factor of 4 – 10. Similarly, Solomon et al. (1997) conclude from comparisons of the dynamical and gas mass derived from the FIR emission and the CO, that the Galactic conversion factor between the CO luminosity,  $L_{\text{CO}}$ , and the molecular gas mass,  $M_{\text{H}_2}$ , overestimates  $M_{\text{H}_2}$  by a factor of about 5. This conclusion is supported by a better determination of the dynamical mass of a sample of ULIRGs using high angular resolution observations made with the Plateau de Bure interferometer (Downes & Solomon 1998).

In this paper we report on observations of the 850  $\mu\text{m}$  emission for a sample of 19 LIRGS galaxies using the submillimetre-wave continuum bolometer array, SCUBA (Holland et al. 1999), at the JCMT<sup>†</sup>. The aim of these observations has been twofold: firstly, to study the dust emission from a selection of galaxies believed to have an ISM quite different to that of our own Galaxy, and secondly, to compare the molecular gas mass derived from the dust emission at 850  $\mu\text{m}$  with that derived from CO measurements in order to assess whether the assumptions on which both methods rely are valid for galaxies spanning a wide range of different star formation activities. The large field of view of SCUBA enables us to include any extended dust emission and to measure its size. In this way we are able to avoid the limitations of previous studies made with single-pixel bolometers (e.g. Andreani & Franceschini 1996, Lisenfeld et al. 1996).

<sup>†</sup> The James Clerk Maxwell Telescope is operated by The Joint Astronomy Centre on behalf of the Particle Physics and Astronomy Research Council of the United Kingdom, the Netherlands Organization for Scientific Research, and the National Research Council of Canada.

## 2 SAMPLE AND OBSERVATIONS

The sample consists of 19 galaxies selected from the subsample of the Bright IRAS galaxies observed in CO(1-0) with the NRAO 12m telescope by Sanders et al. (1991). The combination of the large CO beam (55") and the small optical diameter of our sample means that no CO emission has been missed. The galaxies were selected to cover a wide range of infrared luminosities ( $7.6 \cdot 10^{10} L_{\odot} < L_{\text{IR}} < 3.1 \cdot 10^{12} L_{\odot}$ )<sup>‡</sup> and infrared-to-blue-luminosity ratios  $L_{\text{IR}}/L_{\text{B}}$  ( $2 < L_{\text{IR}}/L_{\text{B}} < 80$ ), thus sampling a wide range of luminosities and star formation activities (as traced by  $L_{\text{IR}}/L_{\text{B}}$ ).

The galaxies were mapped in service time with SCUBA at the JCMT between July 1997 and April 1998. The 16-jiggle mode was used for the observations to obtain fully sampled maps at 850  $\mu\text{m}$ ; the weather conditions were too poor in order to make use of the 450  $\mu\text{m}$  data that was obtained parallelly. The chop throws ranged between 60" and 120" (see Table 1) and the integration time per map was between 15 and 70 minutes. The sky opacity at 850  $\mu\text{m}$  varied between 0.2 and 0.45. The data were reduced using the software package SURF (Jenness 1998). The data were flat-fielded, extinction-corrected and despiked, with bad bolometers and bad channels removed prior to rebinning and flux calibration. Flux calibration was achieved using Uranus and the secondary calibrators CRL 618, IRC+10216, OH231.8. The conversion factor between volts and Jy was found to be quite consistent over different nights, with an average value of  $264 \pm 19$  Jy/V.

## 3 RESULTS

Listed in Table 1 are the measured 850  $\mu\text{m}$  fluxes (column 6) together with 12, 25, 60 and 100  $\mu\text{m}$  IRAS fluxes taken from the IRAS Faint Source Catalog (1990). The flux errors given in column 6 represent the noise in the maps,  $\sigma_{\text{n}}$ . The total error,  $\sigma$ , used for the model fitting, takes additional account of the estimated calibration error,  $\sigma_{\text{cal}}$ , of an estimated 20 per cent:  $\sigma^2 = \sigma_{\text{n}}^2 + \sigma_{\text{cal}}^2$ . Fourteen of the nineteen galaxies were detected at 850  $\mu\text{m}$ , with  $3\sigma_{\text{n}}$  upper limits of between 50 and 200 mJy obtained for the remaining five galaxies. These upper limits have been computed under the assumption that the angular size of the galaxy is small compared to the beam; if considerable extended emission is present, the total fluxes could be higher.

We have found extended emission for NGC 5653 and NGC 5936. For NGC 5653 a Gaussian fit yielded a Full Width Half Maximum (FWHM) of 17", whereas the shape of NGC 5936 is rather irregular with a maximum diameter of about 40". In the case of NGC 1614 and NGC 3110 there could be extended emission present, but the noise level of our data is not low enough in order to definitely confirm this. For the other galaxies we determined the source sizes to have a FWHM of less than 8". The flux at 850  $\mu\text{m}$  was determined as the integrated flux over the source extension.

<sup>‡</sup> We follow the definition of IR luminosity of Sanders & Mirabel (1996) with  $L_{\text{IR}} = L(8 - 1000 \mu\text{m}) = 5.6 \cdot 10^5 D_{\text{Mpc}}^2 (13.48 F_{12} + 5.16 F_{25} + 2.58 F_{60} + F_{100})$  where the fluxes are in Jy.

**Table 1.** FIR and submillimetre data

(1) Name	(2) F <sub>12μm</sub> [Jy]	(3) F <sub>25μm</sub> [Jy]	(4) F <sub>60μm</sub> [Jy]	(5) F <sub>100μm</sub> [Jy]	(6) F <sub>850μm</sub> <sup>(a)</sup> [mJy]
NGC 1614	1.44	7.29	32.3	32.7	110 ± 21 <sup>(3)</sup>
NGC 3110	0.59	1.04	10.7	19.2	144 ± 27 <sup>(2)</sup>
NGC 4194	0.83	4.31	21.4	25.9	113 ± 22 <sup>(1)</sup>
NGC 4418	0.93	9.32	40.7	32.8	290 ± 13 <sup>(1)</sup>
NGC 5135	0.64	2.40	16.9	28.6	182 ± 20 <sup>(1)</sup>
NGC 5256	0.23	0.98	7.3	11.1	71 ± 7 <sup>(1)</sup>
NGC 5653	0.70	1.29	11.0	20.8	176 ± 24 <sup>(1)</sup>
NGC 5936	0.48	1.26	8.5	16.1	147 ± 32 <sup>(1)</sup>
NGC 6240	0.56	3.42	22.7	27.8	168 ± 10 <sup>(3)</sup>
Arp 193	0.26	1.36	15.4	25.2	104 ± 16 <sup>(1)</sup>
Arp 220	0.48	7.90	112.0	114.0	792 ± 26 <sup>(1)</sup>
Mrk 231	1.87	8.66	32.0	30.3	126 ± 13 <sup>(1)</sup>
Mrk 273	0.24	2.28	21.7	21.4	104 ± 10 <sup>(1)</sup>
Zw 049	0.08	0.77	20.8	29.4	180 ± 16 <sup>(1)</sup>
IC 2810	0.19	0.58	5.9	10.3	< 52 <sup>(2)</sup>
NGC 1667	0.43	0.68	5.9	14.7	< 66 <sup>(3)</sup>
NGC 2623	0.21	1.74	23.1	27.9	< 198 <sup>(3)</sup>
IRAS 0519	0.73	3.44	13.7	11.4	< 110 <sup>(1,3)</sup>
IRAS 1212	0.11	0.52	8.5	10.0	< 52 <sup>(1)</sup>

(a) The quoted flux error is estimated from the noise across the SCUBA maps,  $\sigma_n$ . The upper limits are  $3\sigma_n$ . The chop throws used are (1) 60", (2) 100" and (3) 120".

#### 4 DUST EMISSION

We have fitted simple models to the observed 850  $\mu\text{m}$  flux densities together with the IRAS flux densities at 100  $\mu\text{m}$ , 60  $\mu\text{m}$ , and, in the case of the two-temperature model, additionally at 25  $\mu\text{m}$ . The fits are made with only three or four data points and so it is not possible to constrain a model with more than this number of free parameters. Therefore, a number of assumptions are made about the dust. In the first model we assume that the dust is at a single physical temperature, and that the emission is optically thin. In the second model we fixed the dust emissivity law, and adopted a two-component optically thin dust model, while in the third, we explored an optically thick model. In each case the data fits were made by varying the free model parameters and searching for the minimized  $\chi^2$ .

##### 4.1 Optically thin, single-temperature emission

We have used a single-temperature, optically thin dust model given by

$$S_\lambda = B_\lambda(T)\tau_\lambda \propto B_\lambda(T)k_\lambda \quad (1)$$

to fit the 850, 100 and 60  $\mu\text{m}$  flux densities, where  $B_\lambda(T)$  is the Planck function,  $\tau_\lambda$  is the dust opacity and  $k_\lambda$  the dust absorption coefficient. At wavelengths long compared to the physical grain size ( $\lambda \gg a$ , with  $a$  the grain size), the dust absorption coefficient can be parameterized by

$$k_\lambda \propto \lambda^{-\beta}. \quad (2)$$

The wavelength dependence of  $k_\lambda$  is not well known, and depends on the physical composition of the dust. Theoretical

arguments suggest values of  $\beta$  between 1 and 2 (see Tielens & Allamandola 1987). Models of interstellar dust that are both astronomically realistic in composition, and able to reproduce the observed dust extinction and emission curves, predict  $\beta \simeq 2$  (e.g. Draine & Lee 1984, Ossenkopf & Henning 1994, Krügel & Siebenmorgen 1994). The value of  $\beta$  becomes somewhat lower ( $\beta \approx 1.5$ , Désert, Boulanger & Puget 1990) if stochastic heating of small grains to high temperatures is taken into account. Even smaller values of  $\beta \simeq 0.4$  are predicted/observed in the atmospheres of Vega-type stars, where large dust grains that do not satisfy the condition of  $\lambda \gg a$  even at submillimetre wavelengths can form (Krügel & Siebenmorgen 1994).

In Fig. 1 we show the data for the galaxies together with the best model fits. Three different curves are shown: the solid line depicts the dust emission model with the best-fit  $\beta$  and  $T$  while the dotted and dashed lines show the best-fit  $T$  models with  $\beta$  of 1 and 2 respectively. The dust-temperatures derived for the case of variable  $\beta$  lie between 30 and 60 K. When only upper limits at 850  $\mu\text{m}$  were measured, the fits were made using a fixed  $\beta$  and the 60 and 100  $\mu\text{m}$  flux densities only. The results for  $\beta$  and  $T$  are not significantly different if an alternate wavelength dependence of  $k_\lambda$  is used at short wavelengths ( $k_\lambda \propto \lambda^{-1}$  for  $\lambda < 250\mu\text{m}$ , Hildebrand 1983).

The dust emission from all galaxies is well-fit by the single-temperature dust model, with  $1 \lesssim \beta < 2$ . The distribution of the values of the best-fit  $\beta$  as a function of  $L_{\text{IR}}/L_{\text{B}}$  are shown in Fig. 2, where the error bars on  $\beta$  have been estimated by performing fits with the 850  $\mu\text{m}$  flux plus/minus  $\sigma$ . The ratio  $L_{\text{IR}}/L_{\text{B}}$  is frequently used as an indicator for the star formation activity since  $L_{\text{B}}$  and  $L_{\text{IR}}$  reflect the average star formation rates during the last  $\simeq 3 \times 10^9$  and  $\simeq 10^8$  yr, respectively. Starburst galaxies have a much higher ratio ( $L_{\text{IR}}/L_{\text{B}} \simeq 1-100$ ) than normal galaxies ( $L_{\text{IR}}/L_{\text{B}} < 1$ ). The interpretation of  $L_{\text{IR}}/L_{\text{B}}$  as an indicator of star formation has to be made with caution, as the ratio is also affected by the amount of dust present (Calzetti et al. 1995). No trend of  $\beta$  with  $L_{\text{IR}}/L_{\text{B}}$  is seen. The majority of galaxies in the sample have values of  $\beta$  around 1.5 or higher, in agreement with the predictions of astronomical models (see above). The only exceptions are of Arp 220 and NGC 4418 which have a lower  $\beta$ , close to 1.

These low values of  $\beta$  could be an indication of very different dust properties, for example, a higher proportion of very small or very large grains. Although we cannot exclude this possibility, it is not clear why these two galaxies, that at face value do not differ substantially from the other members of the sample, should possess dust grains with different properties. A more plausible explanation is that some of the simple assumptions on which our fits are based are not correct. In the following subsection we explore the validity of these assumptions.

##### 4.2 Optically thin, multi-temperature emission

The modeling of the previous section was based on the assumption that all the dust was at a single dust temperature. This is quite simplistic as in principle the dust will be at a range of temperatures that depends on the local radiation field. Observations of spiral galaxies have shown that indeed at least two components, a warm and a cold one ( $T \lesssim 20\text{K}$ ),

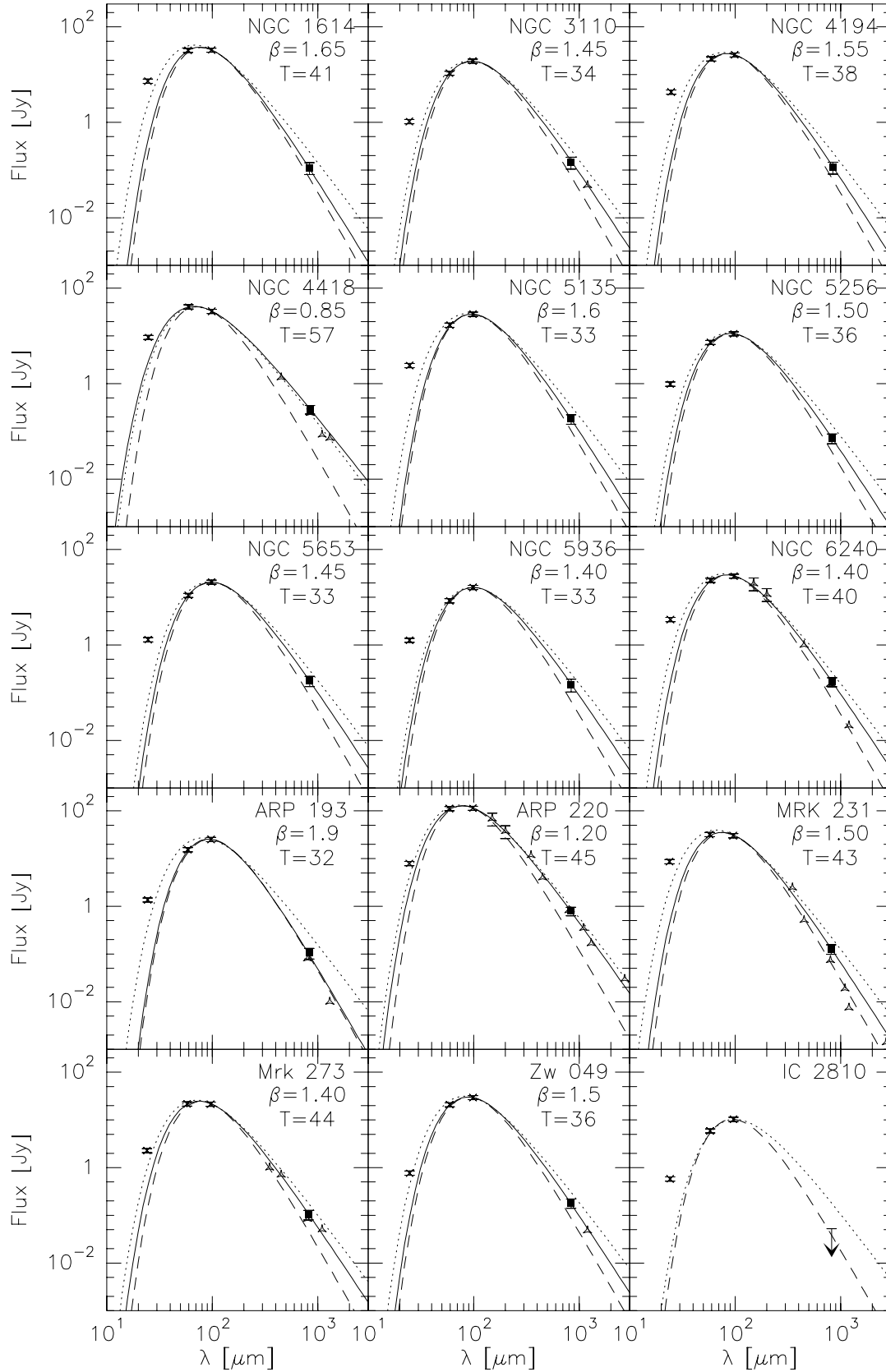


**Figure 1.** The dust emission spectrum for the galaxies. The filled squares are our 850  $\mu\text{m}$  measurements, the crosses are IRAS data and the open triangle data taken from the literature (Braine & Dumke 1998; Carico et al. 1992; Downes & Solomon 1998; Klaas et al. 1997; Lisenfeld et al. 1996; Rigopoulou et al. 1996; Roche & Chandler 1993; Scoville et al. 1991). The fits are done taking into account the data at 60, 100 and, in case of detection, 850  $\mu\text{m}$ . The dashed line is a fit with  $\beta = 2$ , the dotted line for  $\beta = 1$  and in the full line the fit is performed also for  $\beta$ . The best-fit value for  $\beta$  and for the dust temperature  $T$  in this case are written in the graphs.

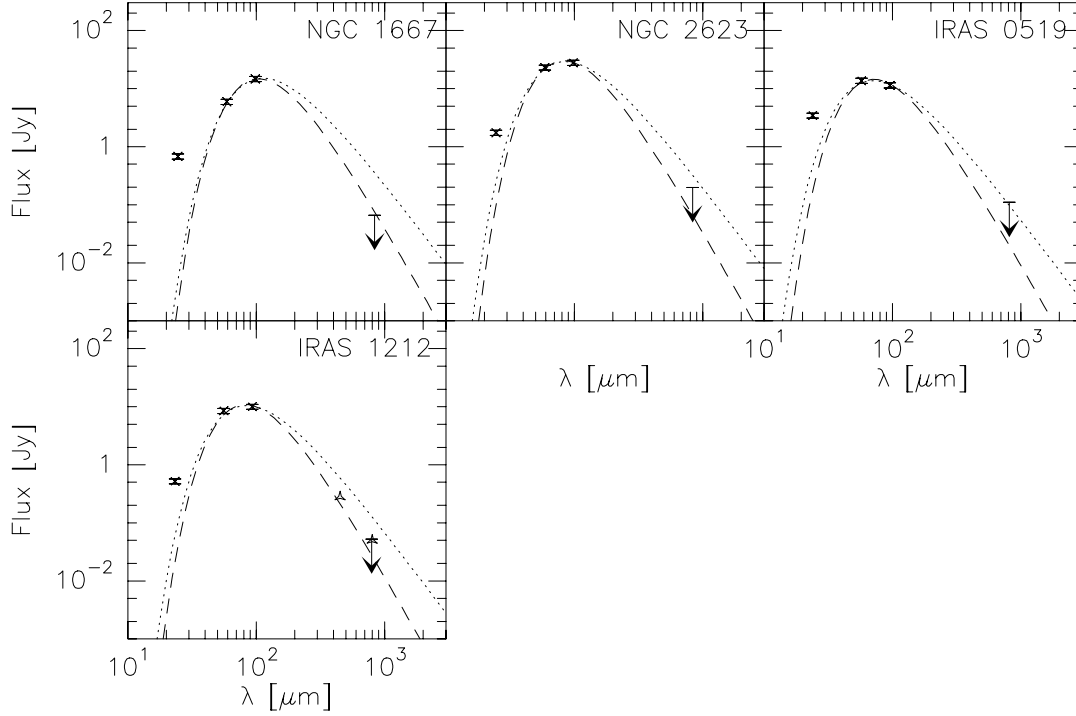
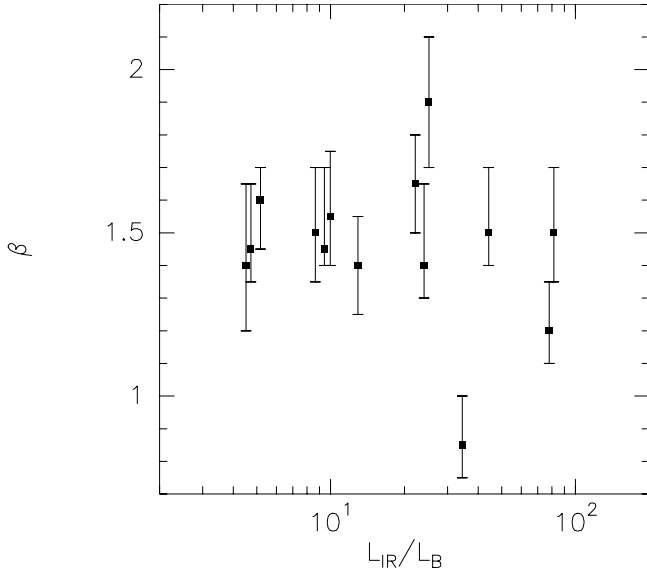


Figure 1 – continued



**Figure 2.** The exponent of the wavelength dependence of the extinction coefficient,  $\beta$ , is shown as a function of  $L_{\text{IR}}/L_{\text{B}}$ .

are necessary to explain the dust emission spectrum from FIR to millimetre wavelengths (e.g. Guélin et al. 1993, Chini et al. 1995, Alton et al. 1998). As a first approximation to a more realistic model, we have applied a two-temperature fit to the data, with  $\beta = 2$ .

In Fig. 3 we show the results of a two-temperature model fit to the 25, 60, 100 and 850  $\mu\text{m}$  fluxes for a selection of the galaxies in the sample: Arp 220 and NGC 4418 have been taken as examples of galaxies with low values of best-fit  $\beta$ , while NGC 6240 and Arp 193 are examples with higher values of  $\beta$  (1.4 and 1.9, respectively). The data points are

reasonably well-fit for these as well as other galaxies not shown. The discrepancy between the model and some of the data points, e.g. with the ISO fluxes at 150 and 200  $\mu\text{m}$  of Arp 220 (Klaas et al. 1997), could easily be improved using more temperature components.

The high 850/60 and 850/100  $\mu\text{m}$  flux ratios observed in Arp 220 and NGC 4418 necessitate the presence of large amounts of cold dust. The temperature of the second dust component needed to model the emission from these two galaxies is  $T_c \simeq 21 - 22$ , rather colder than that typically found for active galaxies ( $T = 33$  K, Chini et al. 1995). In a more realistic multi-temperature model using more than 2 temperature components, the temperature of the coldest dust component would be even lower. This is surprising as, a priori, it is unlikely that Arp 220 and NGC 4418 have colder dust than other galaxies in the sample, particularly given that they show among the highest values of  $L_{\text{IR}}/L_{\text{CO}}$ <sup>§</sup>.

### 4.3 Optically thick dust emission

As discussed in the introduction, there is mounting evidence to suggest that the dust opacity in LIRGs is high. To investigate the effects of dust opacity, the data at 60, 100 and

<sup>§</sup> The ratio  $L_{\text{IR}}/L_{\text{CO}}$  can be interpreted as a rough measure of the dust temperature using the following argument:  $L_{\text{CO}}$  is proportional to the brightness temperature,  $T_b$ , of the molecular gas in the galaxy. If we assume that  $T_b = T$ , the temperature of the dust, and take  $L_{\text{CO}}$  as a measure of both the gas and dust mass (assuming a fixed gas-to-dust ratio), we obtain after reordering equation 7 and integrating over wavelengths,  $L_{\text{IR}}/L_{\text{CO}} \propto \int B_\lambda(T) k_\lambda d\lambda / T \propto T^5$ , for optically thin dust emission with  $\beta = 2$ . In contrast, if the dust is optically thick, then this relation changes to  $L_{\text{IR}}/L_{\text{CO}} \propto \int B_\lambda(T) d\lambda / T \propto T^3$ . In both cases, a high  $L_{\text{IR}}/L_{\text{CO}}$  is indicative of a high dust temperature.

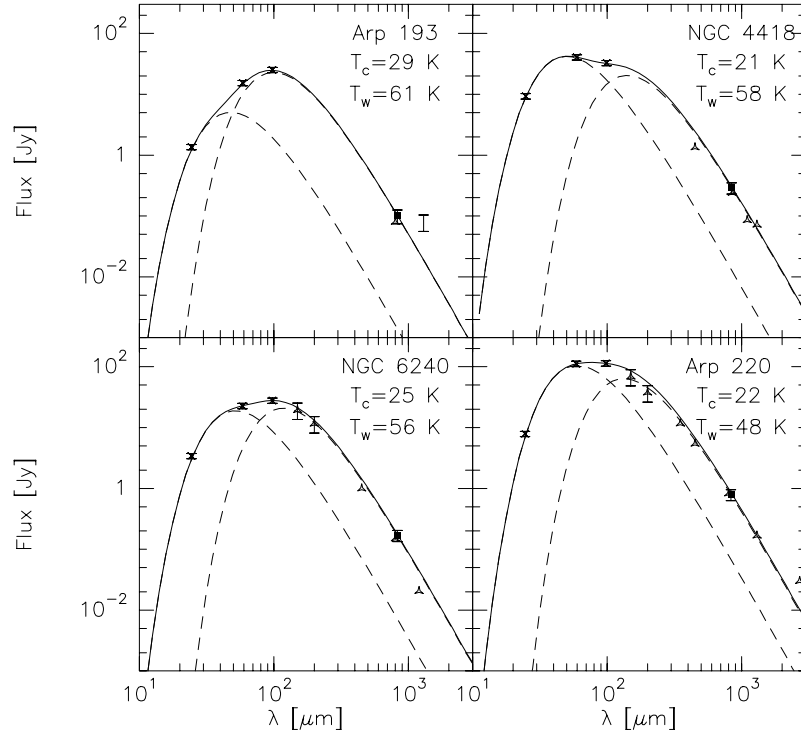


**Figure 3.** The dust emission fitted with a two-temperature model for  $\beta = 2$ . The temperature of the cold ( $T_c$ ) and of the warm ( $T_w$ ) dust component are indicated.

850  $\mu\text{m}$  were fit using a dust emission model with a finite optical depth given by:

$$S_\lambda = B_\lambda(T) (1 - e^{-\tau_\lambda}), \quad (3)$$

where

$$\tau_\lambda = \tau_{100\mu\text{m}} (100\mu\text{m}/\lambda)^\beta. \quad (4)$$

The model fits for the two galaxies Arp 220 and NGC 4418 are shown in Fig. 4, where the dust temperature and opacity have been optimized for fixed values of  $\beta$  (2, 1.8, 1.6). For  $\beta = 2$ , the derived dust opacities are high and in Arp 220 the fit is only marginally consistent with the observed 150 and 200  $\mu\text{m}$  fluxes. The fit improves with decreasing  $\beta$ , with the derived opacities becoming consistent with independent estimates of other authors.

We conclude that the high 850/60 and 850/100  $\mu\text{m}$  flux ratios of Arp 220 and NGC 4418 relative to the rest of the sample is consistent with a high dust opacity.

The models discussed are very simplistic, and the true physical situation is most likely a combination of both a multiple-component dust temperature and a high dust opacity: a high dust opacity would result in the dust being shielded from the heating radiation, resulting in cooler dust components in regions further from the radiation source.

## 5 DUST AND GAS MASSES

The second objective of the project was to compare the molecular gas masses of the sample derived using the two standard methods (a) from CO measurements (b) from dust measurements.

### 5.1 Molecular gas mass derived from the CO emission

CO luminosities were calculated using CO(1-0) measurements taken from the literature. From these, we derived molecular gas masses using:

$$M_{\text{CO}} = 4.78 L_{\text{CO}} [M_\odot] \quad (5)$$

(Sanders et al. 1991), with  $L_{\text{CO}}$ , the CO luminosity in  $\text{K km s}^{-1} \text{pc}^2$ , given by

$$L_{\text{CO}} = 26.55 D^2 I_{\text{CO}} \Theta_B^2 [\text{K km s}^{-1} \text{pc}^2] \quad (6)$$

where  $I_{\text{CO}}$  is the integrated main beam temperature in K,  $D$  is the source distance in Mpc, and  $\Theta_B^2$  the half power beam width (HPBW) of the beam in  $\text{arcsec}^2$ . The quantity  $I_{\text{CO}}$  has been taken from Sanders et al. (1991)<sup>¶</sup> for the majority of galaxies, however, in the case of Arp 220, Arp 193, Mrk 231, Mrk 273 and NGC 6240 data from Solomon et al. (1997) (taken with IRAM 30m telescope) were used instead. The fluxes measured by Solomon et al. (1997) for three of these galaxies (Arp 220, Mrk 231 and Arp 193) are a factor of two higher than those measured by Sanders et. al (1991). The origin of this difference is unclear. We have adopted the values measured by Solomon et al. (1997) because of the higher signal-to-noise and better overall quality of their observed spectra. The values for  $L_{\text{CO}}$  and  $M_{\text{CO}}$  are tabulated in columns 4 and 7 of Table 2 respectively. The error in  $M_{\text{CO}}$  is determined by the error in  $I_{\text{CO}}$ , which we have estimated

<sup>¶</sup> We have transformed the  $T_R^*$  temperature scale used in Sanders et al. (1991) to  $T_{\text{mb}}$  by multiplication with  $\eta_{\text{moon}}/\eta_B = 1.19$  (Sanders et al. 1991)

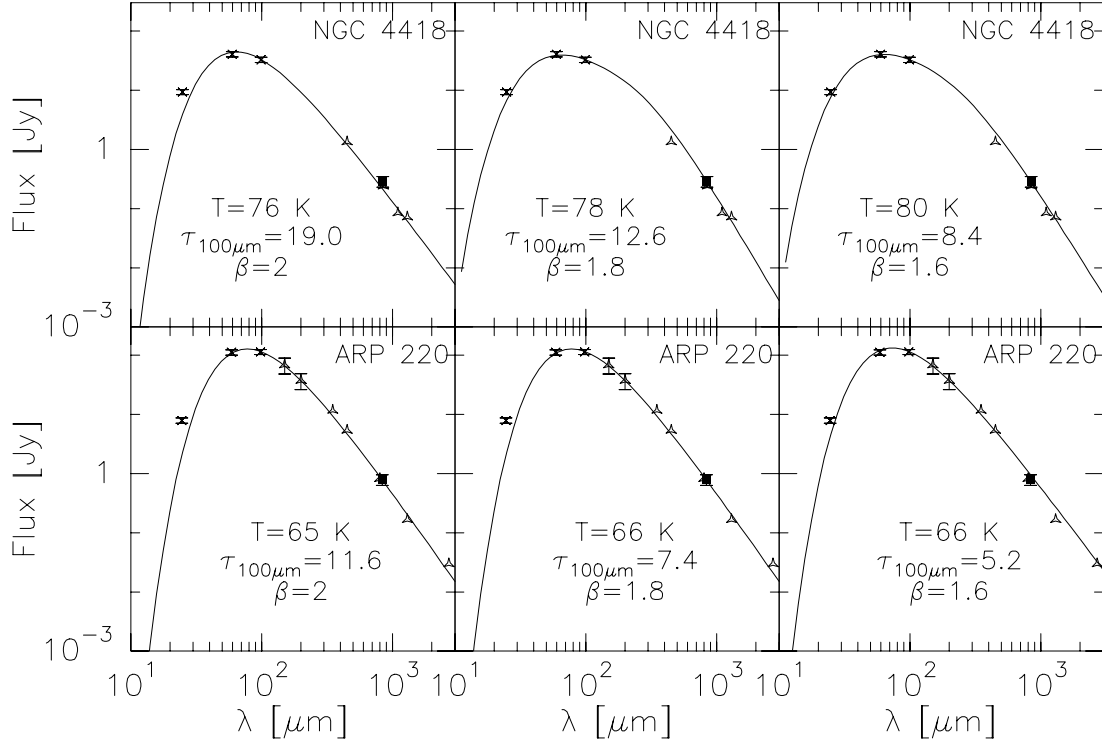


**Figure 4.** The dust emission, taking into account a finite dust opacity, according to eqs. 3 and 4, is shown for Arp 220 and NGC 6240 for different values of  $\beta$ . The best-fit value for the dust opacity at 100  $\mu\text{m}$ ,  $\tau_{100\mu\text{m}}$ , and the corresponding dust temperature  $T$  are indicated.

by comparing the data used here with other published CO data (Young et al. 1995), where we find CO(1-0) fluxes for 11 galaxies of our sample. On average, there is a difference of about 25 per cent between the two data sets which we adopt as the uncertainty in  $I_{\text{CO}}$ .

## 5.2 Molecular gas mass derived from the dust emission

The molecular gas mass can be calculated from the 850  $\mu\text{m}$  emission:

$$M_{850\mu\text{m}} = \frac{D^2 S_{850\mu\text{m}}}{B_{850\mu\text{m}}(T) k_{850\mu\text{m}}} \quad (7)$$

where optically thin dust emission at 850  $\mu\text{m}$  is assumed (this is correct even for the high dust opacities estimated in the previous section).

We have adopted temperatures derived in the best-fit  $\beta$  models. We have used the value for  $k_{850\mu\text{m}}$  given by Hildebrand (1983) which, for  $\beta = 2$  and for a gas-to-dust mass ratio of 150, is  $k_{850\mu\text{m}} = 0.0058 \text{ cm}^2 \text{ g}^{-1}$ . For comparison with other authors, this value can be extrapolated to 1.3 mm, where we obtain (for  $\beta = 2$ )  $k_{1.3\text{mm}} = 0.0025 \text{ cm}^2 \text{ g}^{-1}$ . Based on extensive simulations of dust emission and absorption Krügel, Steppe & Chini (1990) estimate  $k_{1.3\text{mm}} = 0.003 \text{ cm}^2 \text{ g}^{-1}$ . Mezger, Wink & Zylka (1990) suggest a value of  $k_{1.3\text{mm}} = 0.0013 b z \text{ cm}^2 \text{ g}^{-1}$ , where  $b$  is a measure of the dust environment and  $z$  is the metallicity. Adopting a value of  $b = 1.9$  for moderately dense gas yields (for  $z = 1$ ) a value of  $k_{1.3\text{mm}} = 0.0025 \text{ cm}^2 \text{ g}^{-1}$ , which matches the value adopted in this paper. In contrast, the “standard” dust model of Draine & Lee (1984) gives a somewhat lower value

of  $k_{1.3\text{mm}} = 0.0015 \text{ cm}^2 \text{ g}^{-1}$ , which has been found to agree with observational comparisons between dust extinction at IR wavelength and dust emission at FIR/mm wavelength in dense Galactic molecular cloud cores (Kramer et al. 1998, Lehtinen et al. 1998).

The most significant uncertainty in this method, apart from  $k_{850\mu\text{m}}$ , is the dust temperature. The error in the dust temperature can be estimated by comparing the temperatures derived in the different models (optically thin/thick, single temperature or various temperature components) used here, which differ by about 50 per cent. At submillimetre wavelengths the Planck function depends linearly on the dust temperature, so this uncertainty in the dust temperature produces an error in  $M_{850\mu\text{m}}$  of 50 per cent also. Adding to this quadratically the measurement error of the 850  $\mu\text{m}$  flux densities (on average 25 per cent), we estimate an error of 55 per cent for  $M_{850\mu\text{m}}$ .

## 5.3 Comparison between the two masses

In Fig. 5 we show the comparison between the molecular gas mass derived from the CO emission,  $M_{\text{CO}}$ , and the molecular gas mass derived from the 850  $\mu\text{m}$  continuum,  $M_{850\mu\text{m}}$ .  $M_{\text{CO}}$  is systematically higher than  $M_{850\mu\text{m}}$ . A good correlation (correlation coefficient  $r = 0.82$ ) exists between the two quantities, spanning nearly 2 orders of magnitude.

In Fig. 6 we have plotted the ratio between the molecular gas mass derived using the two alternative methods as a function of  $L_{\text{IR}}$  and as a function of  $L_{\text{IR}}/L_{\text{B}}$  to see whether there is any trend with luminosity or the star formation activity. The error of  $M_{\text{CO}}/M_{850\mu\text{m}}$  is the root of the sum of the squares of the errors in  $M_{\text{CO}}$  and  $M_{850\mu\text{m}}$ , and so ap-

**Table 2.** Luminosities and gas masses

(1)	(2)	(3)	(4)	(5)	(6)	(7)	(8)	(9)	(10)
Name	Distance	$L_{\text{IR}}$	$L_{\text{CO}}$	$L_{\text{B}}$	$M_{850\mu\text{m}}$	$M_{\text{CO}}$	$\frac{L_{\text{IR}}}{L_{\text{CO}}}$	$\frac{L_{\text{IR}}}{L_{\text{B}}}$	$\frac{M_{\text{CO}}}{M_{850\mu\text{m}}}$
	[Mpc]	[ $10^{11} L_{\odot}$ ]	[ $10^8 L'$ ]	[ $10^{10} L_{\odot}$ ]	[ $10^9 M_{\odot}$ ]	[ $10^9 M_{\odot}$ ]			
NGC 1614	62.3	3.8	31.9	1.7	2.9	15.3	117.8	22.2	5.2
NGC 3110	69.3	1.6	59.7	1.7	5.9	28.6	27.1	9.4	4.8
NGC 4194	41.4	1.1	6.7	1.1	1.4	3.2	163.6	10.0	2.3
NGC 4418	34.2	1.3	5.3	0.4	1.6	2.5	247.2	34.4	1.6
NGC 5135	56.9	1.7	34.4	3.3	5.2	16.4	49.2	5.2	3.2
NGC 5256	115.9	2.9	63.0	3.3	7.6	30.1	45.6	8.7	3.9
NGC 5653	54.4	1.1	15.0	2.3	4.5	7.2	72.1	4.7	1.6
NGC 5936	59.0	1.0	19.0	2.2	4.4	9.1	52.4	4.5	2.0
NGC 6240	100.9	6.4	90.4	4.9	12.1	43.2	70.4	12.9	3.6
Arp 193	97.8	4.0	44.3	1.6	9.1	21.2	91.3	25.2	2.3
Arp 220	79.2	15.8	88.0	2.0	30.0	42.0	179.9	78.2	1.4
Mrk 231	173.9	31.0	85.6	7.0	24.2	40.9	361.8	44.2	1.7
Mrk 273	153.8	12.2	57.8	5.1	15.3	27.6	211.8	24.1	1.8
Zw 049	52.3	1.3	8.9	0.2	3.8	4.3	149.9	81.5	1.1
IC 2810	140.5	3.2	54.8	3.4	< 10.0	26.2	57.6	9.3	> 2.6
NGC 1667	58.9	0.8	12.3	3.4	< 2.5	5.9	62.3	2.3	> 2.3
NGC 2623	76.1	3.2	26.6	2.8	< 9.4	12.7	121.1	11.7	> 1.4
IRAS 0519	167.5	11.7	69.8	—	< 21.2	33.4	167.4	—	> 1.6
IRAS 1212	293.3	16.7	123.5	—	< 36.7	59.0	135.1	—	> 1.6

(2) Distance taken from Sanders et al. (1991), based on  $H_0 = 75 \text{ km s}^{-1} \text{ Mpc}^{-1}$  and taking into account the Virgocentric flow.

(3)  $L_{\text{IR}} = L(8 - 1000\mu\text{m}) = 5.6 \cdot 10^5 D_{\text{Mpc}}^2 (13.48F_{12} + 5.16F_{25} + 2.58F_{60} + F_{100})$  where the flux is in Jy (Sanders & Mirabel 1996).

(4)  $L' = K \text{ km s}^{-1} \text{ pc}^2$ ;  $L_{\text{CO}}$  is calculated according to eq. (6).

(5) Calculated from  $B_{\text{T}}^0$ , taken from de Vaucouleur et al. (1991), except for Zw 049 and NGC 3110 which have been taken from Lehnert & Heckman (1995) and Lutz (1992), respectively.

(6) Molecular gas mass estimated from the CO emission, calculated according to eq. (5).

(7) Molecular gas mass estimated from the dust emission, calculated according to eq. (7).

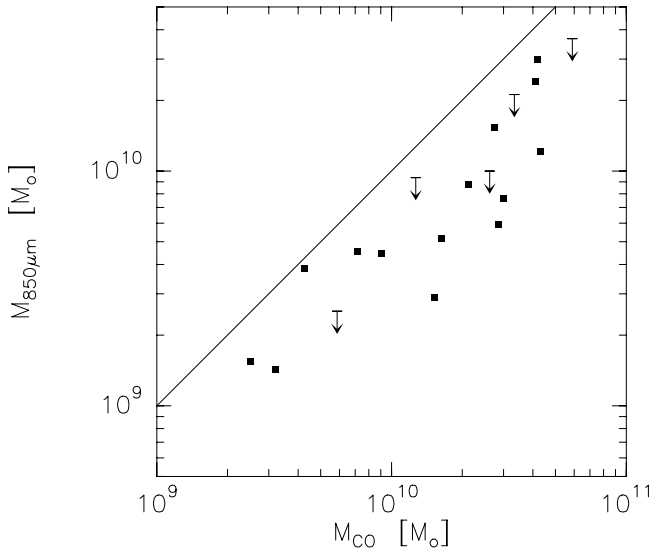


**Figure 5.** The molecular gas mass derived from the CO-luminosity,  $M_{\text{CO}}$ , and the molecular gas mass derived from the dust emission,  $M_{850\mu\text{m}}$ . The diagonal line shows the relation  $M_{\text{CO}} = M_{850\mu\text{m}}$ .

proximately 60 per cent. The average ratio,  $M_{\text{CO}}/M_{850\mu\text{m}}$  is  $2.6 \pm 1.3$ , ignoring upper limits. There is no trend visible for  $M_{\text{CO}}/M_{850\mu\text{m}}$  to vary with  $L_{\text{IR}}$ . There might be a weak anticorrelation in the LIRG sample between  $M_{\text{CO}}/M_{850\mu\text{m}}$  and

$L_{\text{IR}}/L_{\text{B}}$ , but the statistical significance is low and a larger sample size will be needed in order to confirm or refute this anticorrelation.

Also plotted in Fig. 6 are data taken from the literature for other galaxies, including spiral galaxies (NGC 3637, NGC 891) and actively star forming and starburst galaxies (Markarian galaxies, NGC 253). The  $M_{\text{CO}}/M_{850\mu\text{m}}$  ratios for these comparison galaxies have been rederived using the same parameters as for the LIRG sample. The most significant differences between the LIRG sample and these other galaxies is seen in the spiral galaxies NGC 891 (factor of 3.3). The starburst galaxy NGC 253 has about the same ratio as the average of the LIRGs, while the Markarian galaxies have a lower value, possibly due in part to the fact that  $M_{\text{CO}}$  has been derived from the CO(2-1) line emission assuming a ratio of CO(2-1)/CO(1-0) of 1.

We have found for the LIRG sample that the molecular gas mass derived from the CO is higher than that derived from the 850  $\mu\text{m}$ . This confirms the conclusion of other authors, that the standard galactic CO-to-molecular mass conversion factor overestimates the molecular gas mass in LIRGs. The resultant ratio of  $M_{\text{CO}}/M_{850\mu\text{m}}$  is slightly less than that seen in other studies, the results of which suggest that the CO emission overestimates the molecular gas mass by a factor of about 4-5 (Solomon et al. 1997, Downes & Solomon 1998) or more (factor 3-10, Shier et al. 1994, Braine & Dumke 1998). If this higher value is true, it implies that the molecular gas mass derived from the 850  $\mu\text{m}$  flux is also an overestimate. This could be possibly due to a



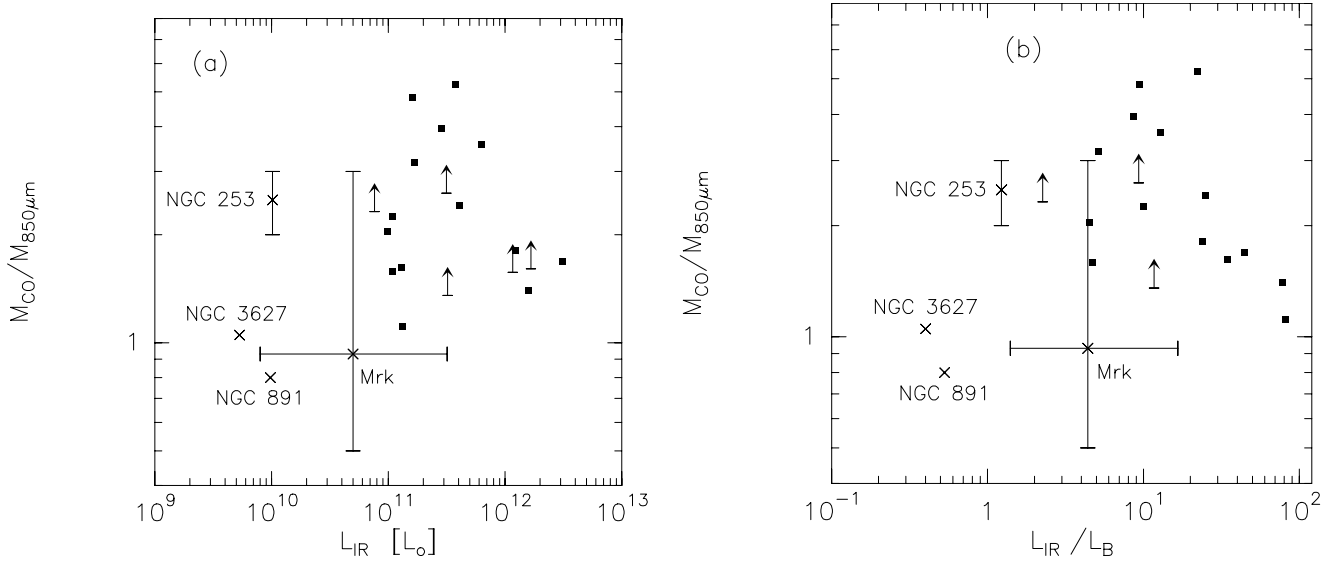


**Figure 6.** The ratio between the molecular gas mass derived from the CO emission and the molecular gas mass derived from the dust emission as a function of  $L_{\text{IR}}$  (a) and of  $L_{\text{IR}}/L_{\text{B}}$  (b) for the LIRG sample (filled squares and arrows). For comparison, data from the literature (crosses) for spiral galaxies (NGC 3627, Sievers et al. 1994; NGC 891, Guélin et al. 1993), Markarian galaxies (“Mrk”, the error bar gives the range for the values in the sample; Chini, Krügel & Steppe 1992), and the starburst galaxy NGC 253 (the error bars give the range of values found in the center and in the disk; Mauersberger et al. 1996) are also included.

higher dust-to-gas mass ratio in these galaxies which could be caused by the higher metallicity produced by intense star formation as seen in galactic nuclei and bulges, for example in the inner part of M 51 (Guélin et al. 1995) and the centre of NGC 253 (Mauersberger et al. 1996).

## 6 CONCLUSIONS AND SUMMARY

We have presented new data at  $850\ \mu\text{m}$  taken with SCUBA at the JCMT for 19 luminous infrared galaxies. Fourteen galaxies were detected at a level of  $5\sigma$  or better. Using the  $850\ \mu\text{m}$  data as well as IRAS fluxes taken from the literature, we have shown that the submillimetre/far-infrared spectral energy distribution for the majority of the sources in the sample is well-described by an optically thin, single temperature dust model, with  $\beta \simeq 1.4 - 2$ . A lower value of  $\beta \simeq 1$  is required to fit the data for two of the galaxies, Arp 220 and NGC 4418.

This difference can be attributed to one, or a combination of: (i) different intrinsic dust properties, (ii) the presence of a large cold-dust component, (iii) high dust opacities. We have discussed the various possibilities and conclude that the most physical explanation is a high dust opacity.

We have compared the molecular gas masses derived from the dust emission to the molecular gas masses derived from the CO emission of our sample. We find, on average, that  $M_{\text{CO}}$  is a factor of 2–3 higher than  $M_{850\ \mu\text{m}}$ . If the CO luminosity indeed overestimates the gas mass by a factor of about 5–10 as indicated by other studies, then the dust emission must also overestimate the gas mass. The most likely reason for this is a higher dust-to-gas mass ratio in LIRGs.

## ACKNOWLEDGMENTS

We would like to thank the staff at the JACH for carrying out the observations, Rob Ivison for useful advices with respect to the data analysis and Loretta Dunne for allowing us to compare our results with observations made in the SCUBA Local Universe and Galaxy survey prior to publication. We would also like to thank the referee for very helpful comments.

## REFERENCES

- Andreani P., Franceschini A., 1996, MNRAS 283, 85
- Alton P.B., Bianchi S., Rand R.J., Xilouris E.M., Davies J.I., Trewheella M., 1998, ApJ, 507, L125
- Bloemen J.B.G.M., Strong A.W., Blitz A.W., et al., 1986, A&A, 154, 25
- Braine J., Dumke M., 1998, A&A, 333, 38
- Carico D.P., Keene J., Soifer B.T., Neugebauer G., 1992, PASP, 104, 1086
- Calzetti D., Bohlin R.C., Kinney A.L., Storchi-Bergmann T., Heckman T. M., 1995, ApJ, 443, 136
- Chini R., Krügel E., Steppe H., 1992, A&A, 255, 87
- Chini R., Krügel E., Lemke R., Ward-Thompson D., 1995, A&A, 295, 317
- de Vaucouleur G., de Vaucouleurs A., Corwin H.G.Jr., Buta R.J., Paturel G., Fouqué P., 1991, Third Reference Catalogue of Bright Galaxies. Springer, Heidelberg
- Désert F.X., Boulanger F., Puget J.L., 1990, A&A, 237, 215
- Downes D., Solomon P.M., 1998, ApJ, 507, 615
- Draine B.T., Lee H.M., 1984, ApJ, 285, 89
- Emerson J.P., Clegg P.E., Gee G., Griffin M.J., Cunningham C.T., Brown L.M.J., Robson E.I., Longmore A.J., 1984, Nat, 311, 237
- Fischer J., Satyapal S., Luhman M.L., Stacey G.J., Smith H.A., Unger S.J., Lord S.D., Greenhouse M.A., Spinoglio L., 1997, Mamon G.A., Xuan Thuan T., Tran Thanh Van J., Proc. of

- XVIIth Rencontre de Moriond, Extragalactic Astronomy in the Infrared. Editions Frontière, Paris, p. 298
- Genzel R., Lutz D., Sturm E., et al., 1998, *ApJ*, 498, 579
- Guélin M., Zylka R., Mezger P.G., Haslam C.G.T., Kreysa E., Lembke R., Sievers A.W., 1993, *A&A*, 279, L37
- Guélin M., Zylka R., Mezger P.G., Haslam C.G.T., Kreysa E., 1995, *A&A*, 298, L29
- Hildebrand R.H., 1983, *QJRAS*, 24, 267
- Holland W.S., Robson E.I., Gear W.K., Cunningham C.R., Lightfoot J.F., Jenness T., Ivison R.J., Stevens J.A., Ade P.A.R., Griffin M.J., Duncan W.D., Murphy J.A., Naylor D.A., 1999, *MNRAS*, 303, 659
- IRAS Faint Source Catalog, 1990, Version 2.0, Moshir M. et al. Infrared Processing and Analysis Center
- Jenness T., 1998, *Starlink User Note* 216.3
- Klaas U., Haas M., Heinrichsen I., Schulz B., 1997, *A&A*, 325, L21
- Kramer C., Alves J., Lada C., Lada E., Sievers A., Ungerechts H., Walmsley M., 1998, *A&A*, 329, L33
- Krügel E., Steppe H., Chini R., 1990, *A&A*, 229, 17
- Krügel E., Siebenmorgen R., 1994, *A&A*, 228, 929
- Lehnert M.D., Heckman T.M., 1995, *ApJS* 97, 89
- Lehtinen K., Lemke D., Mattila K., Haikala L.K., 1998, *A&A*, 333, 702
- Lisenfeld U., Hills R.E., Radford S.J.E., Solomon P.M., 1996, Rottgering H., ed., *Cold gas at high redshift*. Kluwer, Dordrecht, p. 55
- Luhman M.L., Satyapal S., Fischer J., et al., 1998, *ApJ*, 504, L11
- Lutz D., 1992, *A&A*, 259, 462
- Malhorta S., Helou G., Stacey G., et al., 1997, *ApJ*, 491, L27
- Maloney P., Black J.H., 1988, *ApJ*, 325, 389
- Mauersberger R., Henkel C., Wielebinski R., Wiklind T., Reuter H.-P., 1996, *A&A*, 305, 421
- Mezger P.G., Wink J.E., Zylka R., 1990, *A&A*, 228, 95
- Ossenkopf V., Henning Th., 1994, *A&A*, 291, 943
- Rigopoulou D., Lawrence A., Rowan-Robinson M., 1996, *MNRAS*, 278, 1049
- Roche P.F., Aitken D.K., Smith C.H., James S.D., 1986, 218, 19p
- Roche P.R., Chandler C.J., 1993, *MNRAS*, 265, 486
- Sanders D.B., Mirabel I.F., 1996, *ARA&A* 34, 749
- Sanders D.B., Scoville N.Z., Soifer B.T., 1991, *ApJ*, 370, 158
- Sanders D.B., Soifer B.T., Elias J.H., Madore B.F., Matthews K., Neugebauer G., Scoville N.Z., 1988, *ApJ*, 325, 74
- Scoville N.Z., Sargent A.I., Sanders D.B., Soifer B.T., 1991, *ApJ*, 366, L5
- Sievers A.W., Reuter H.-P., Haslam C.G.T., Kreysa E., Lemke R., 1994, *A&A*, 281, 681
- Shier L.M., Rieke M.J., Rieke G.H., 1994, *ApJ*, 433, L9
- Solomon P.M., Downes D., Radford S.J.E., 1992, *ApJ*, 387, L55
- Solomon P.M., Downes D., Radford S.J.E., Barrett J.W., 1997, *ApJ*, 478, 144
- Tielens G.G.G.M., Allamandola L.J., 1987, in Hollenbach D.J., Thronson H.A. Jr., eds., *Interstellar Processes*, Reidel, Dordrecht, p. 397
- Young J.S., Scoville N.Z., 1982, *ApJ* 258, 153
- Young J.S., Xie S., Tacconi L., et al. 1995, *ApJS* 98, 219